Journal of Alloys and Compounds 705 (2017) 183–187

Contents lists available at ScienceDirect

Journal of Alloys and Compounds

journal homepage: http://www.elsevier.com/locate/jalcom

Microstructural characterization of an $\alpha+\beta$ type Ti-5.5Mo-7.2Al-4.5Zr-2.6Sn-2.1Cr alloy during recrystallization annealing

Ran Shi, Guoju Li, Yumeng Xia, Qunbo Fan*, Fuchi Wang, Hongmei Zhang, Xingwang Cheng

School of Materials Science and Engineering, Beijing Institute of Technology, Beijing 100081, China

ARTICLE INFO

Article history:
Received 28 November 2016
Received in revised form
14 January 2017
Accepted 12 February 2017
Available online 16 February 2017

Keywords:
Recrystallization
Three-dimensional morphology
Electron backscatter diffraction
Titanium alloy
Microstructure

ABSTRACT

An $\alpha+\beta$ type titanium alloy was subjected to various periods of recrystallization annealing and the resulting microstructural evolution was characterized. The results revealed that the recrystallization rate of the β phase was higher than that of the α phase, owing to the high strain energy storage of this phase during large deformation forging. Moreover, the recrystallized fraction of both the α and β phases increased with increasing holding time at 740 °C. The recrystallization fraction of the β phase accounted for 70.13% after annealing for 5 h. However, the average grain size remained constant when the recrystallization fraction reached approximately 54%, indicating that further grain refinement was prevented, owing to the high degree of recrystallization. The spatial microstructure which consisted of a globular, homogeneous, and equiaxed α phase dispersed in sub-structured β matrix grains, was characterized via a novel three-dimensional electron backscatter diffraction technique. The grain orientation and morphological parameters, including the equivalent-sphere diameter and number of neighboring grains, were calculated and discussed.

© 2017 Elsevier B.V. All rights reserved.

1. Introduction

Recrystallization affects the microstructure and mechanical properties of materials during forging and annealing and is therefore important from both theoretical and industrial viewpoints [1]. Grain refinement based on continuous dynamic recrystallization (DRX) was realized through multi-directional forging [2,3]. Ning et al. [4,5] developed a unique heat treatment method to produce a gradient microstructure. In those works, multiple passes of forging and annealing treatment resulted in significant grain size refinement, owing to the occurrence of dynamic and static recrystallization.

Furthermore, the microstructure of $\alpha+\beta$ titanium alloys can be improved through severe deformation in the β-phase field and subsequent annealing in the $\alpha+\beta$ phase field [6]. Previous studies [7,8] have shown that the formation of fine grains and the enhancement of high-temperature mechanical properties of titanium alloys subjected to β-forging occur predominantly via DRX. The effect of cooling rate, annealing, and aging temperature (during subsequent heat treatment in the $\alpha+\beta$ phase field) on microstructural evolution and the mechanical properties has been considered in various studies [9–14]. Meng et al. [15] predicted the evolution of the phase fraction (especially of the primary α phase) of two-phase Ti-alloys, with temperature. In addition, Popov et al. [16] determined the effect of heating temperature and holding time on the occurrence of structural and phase transformations in a Ti-6-4 Eli titanium alloy. Jiang et al. [17] considered the effect of recrystallization during annealing of a cold-rolled Ti-6Al-4V alloy and showed that the recrystallization sites of preferred orientations and favorable grain growth played an important role in static recrystallization. When static recrystallization occurs during annealing, the microstructure evolves via competing processes of recovery, nucleation of recrystallization, and grain growth [18]. The influence of holding time at recrystallization temperature on specific characteristics (recrystallization rate and fraction, grain size and phase distribution) has scarcely been investigated. Elucidation of the static recrystallization behavior could aid in the refinement of microstructures.

Therefore, in this work, the microstructural evolution associated with increasing recrystallization-annealing time was characterized via two-dimensional (2D) electron backscatter diffraction (EBSD) analysis. Furthermore, three-dimensional (3D) microstructural

* Corresponding author.
E-mail address: fanqunbo@bit.edu.cn (Q. Fan).

http://dx.doi.org/10.1016/j.jallcom.2017.02.132
0925-8388/© 2017 Elsevier B.V. All rights reserved.

characterization was performed via serial-sectioning using a focused ion beam (FIB) [19–21], field emission scanning electron microscopy (SEM) [22–25] with EBSD, and computer-aided 3D reconstruction and visualization [26]. The precise shape, spatial misorientation and neighboring relationship of the grains, as well as spatial distribution of the phases were obtained via the 3D FIB–EBSD method [27–30].

2. Material and methods

The titanium alloy (Ti-5.5Mo-7.2Al-4.5Zr-2.6Sn-2.1Cr) was prepared by vacuum self-consuming electricity arc melting, followed by rough blooming forging in the β phase field and large deformation forging in the $\alpha+\beta$ phase field. Afterwards, 5 mm × 8 mm × 1 mm specimens were cut from the forged ingot and subsequently solution-treated at 880 °C for 0.5 h. The specimens were then heat-treated at 740 °C for 1 h, 2 h, and 5 h, respectively, and water quenched to retain the high-temperature microstructure. The 2D EBSD measurements were performed at a step size of 0.15 μm using a FEI Nanosem 430 field emission gun scanning electron microscope (SEM, HITACHIS-4800 N, Japan) operated at 20 kV. The samples designated for 2D EBSD were mechanically polished and then electropolished (25 °C, 25 V, ~30 s, solution: 6% $HClO_4$, 34% $CH_3(CH_2)_3OH$, and 60% CH_3OH) to remove the stress from the surface layers.

For serial-sectioning, small (5 mm × 1 mm × 0.5 mm) samples were cut from the water-quenched specimen heat-treated at 740 °C for 5 h. The geometry of the FIB–SEM system requires that the sampling area is positioned close to an edge of the sample. Therefore, the sample was ground to a thickness of ~26 μm (Fig. 1(a)). Measurements were performed on a Zeiss XB1540 crossbeam instrument (Carl Zeiss NTS GmbH, Germany), equipped with a field emission electron column and a Ga^+-ion emitter. For orientation microscopy, a Nordlys F EBSD detector (Oxford Instruments HKL, UK) was positioned on one side of the FIB column (Fig. 1(b)). This positioning allows a 180° rotation of a 16.5° pre-tilted sample holder and, in turn, quick and precise changes between FIB milling (sample at 36°) and EBSD mapping (sample at 70°). The FIB was operated at an accelerating voltage of 30 kV and a milling current of 4 nA. Prior to the experiment, milling was used to create a marker (cross) that was used for drift correction (Fig. 1(c), FIB view). The cross-section was then serial-milled in milling steps of ~100 nm, and the milled region (~15 × 10 μm^2) was examined (Fig. 1(c), SEM view) after each step.

3. Results and discussion

3.1. 2D EBSD analysis

The microstructure development of a 60 × 60 μm^2 region was investigated during recrystallization annealing. Fig. 2 shows the recrystallized-fraction distribution maps of the α and β phases. The recrystallized, sub-structured, and deformed grains are shaded in blue, yellow, and red, respectively. A subgrain is defined by a minimum angle (θ_c) of 1°. If the average misorientation angle within the grain exceeds θ_c, the grain is classified as being "deformed". Some grains consist of subgrains with an internal misorientation of $<\theta_c$, and exhibit a subgrain-to-subgrain misorientation of $>\theta_c$. In this case, the grain is classified as "sub-structured". The remaining grains are classified as "recrystallized". The maps reveal that the grain size of the α phase decreases significantly with increasing annealing time. During the static recrystallization process, the sub-structured matrix resulting from DRX [31] decreases with increasing area of the recrystallized grains.

Fig. 3 shows the distribution histogram and average-grain-size evolution of the α and β phases with annealing time. The α and β phases comprise a negligible fraction (7%) of the deformed grains. Recrystallization fractions of 46.61% and 47.01% of the α phase occur after annealing for 1 h and 2 h, respectively, at 740 °C. The corresponding average grain sizes, 0.86 μm and 0.72 μm, reveal that the

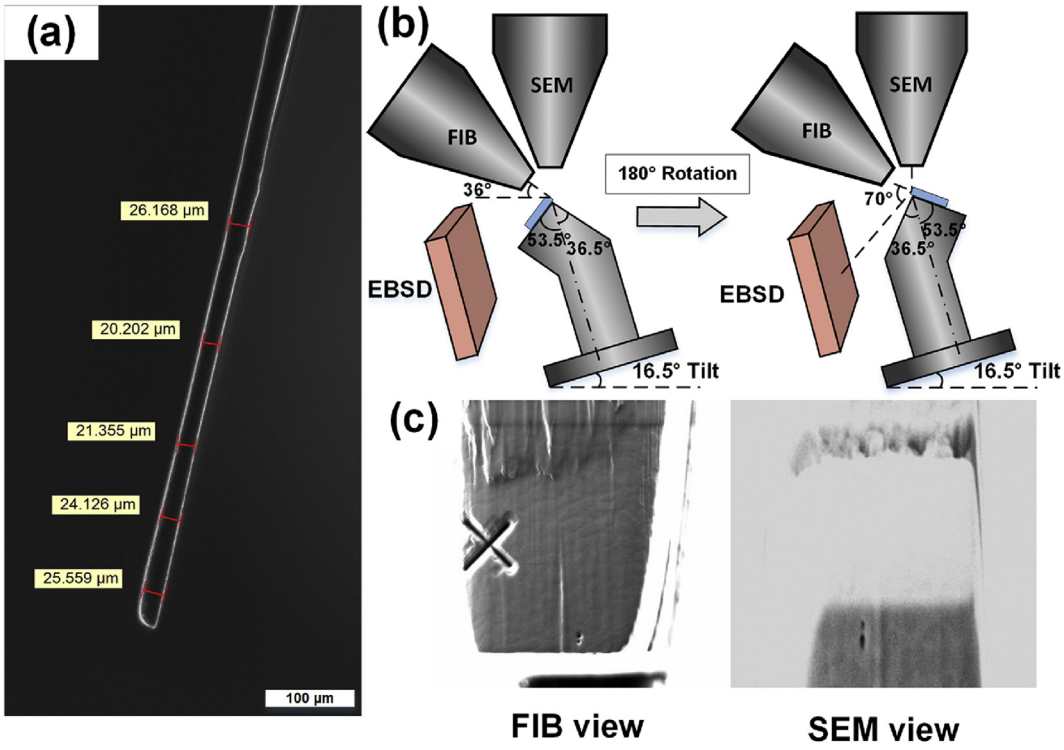

Fig. 1. **(a)** Optical micrographs of the prepared sample; **(b)** schematic of the experimental setup used for the 3D FIB–EBSD method; **(c)** images from FIB and SEM view.

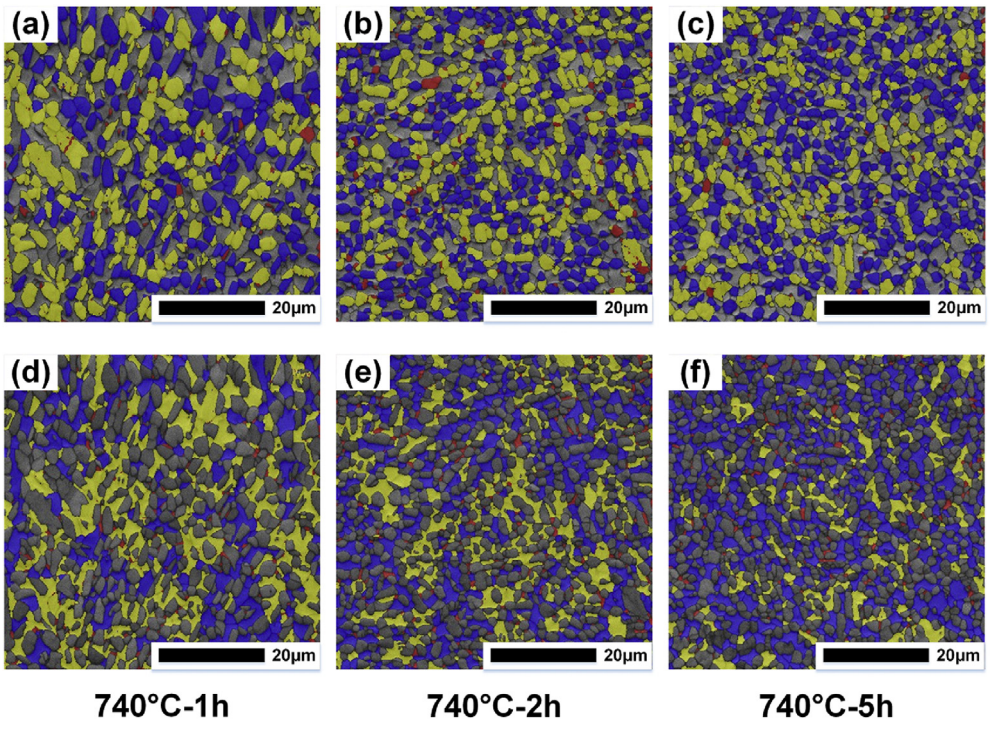

Fig. 2. Recrystallized-fraction distribution maps of the ((**a**)–(**c**)) α phase and ((**d**)–(**f**)) β phase in samples annealed at 740 °C for 1 h, 2 h, and 5 h.

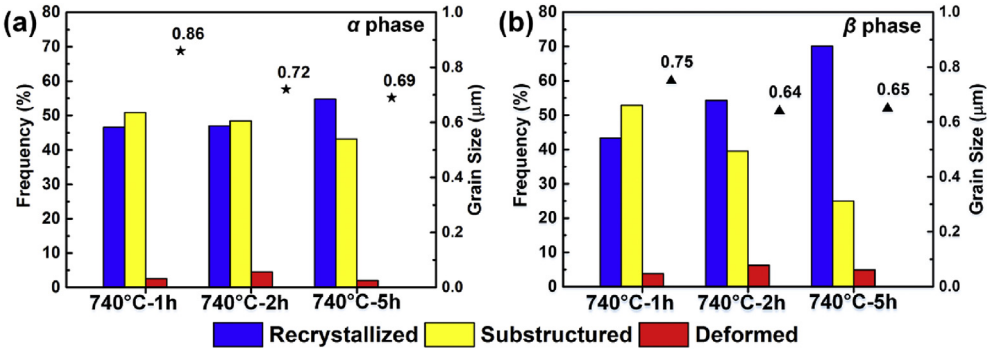

Fig. 3. Recrystallized fraction distribution histogram and average grain size of the **(a)** α phase and **(b)** β phase in samples annealed at 740 °C for 1 h, 2 h, and 5 h.

average grain size decreases during the initial stages of recrystallization. After 5 h at 740 °C, recrystallized grains comprise 54.78% of the α phase and the average grain size drops slightly to a value of 0.69 μm. In the case of the β phase, a recrystallization fraction of 43.35% (comparable to that of the α phase) is obtained after 1 h of annealing. This fraction increases significantly to 54.26% after 2 h. Owing to the large deformation forging in both the β and $\alpha+\beta$ phase fields, the strain energy stored in the β phase is higher than that stored in the α phase. Recrystallization occurs first in these high-stored-energy regions [18] and proceeds at a higher rate than that associated with other regions. After 5 h at 740 °C, recrystallized grains comprise 70.13% of this phase. In addition, the average grain size (0.75 μm) of the β phase after 1 h of annealing decreases to 0.64 μm after 2 h at 740 °C, and remains almost unchanged even after 5 h. This indicates that a critical fraction of recrystallized grains prevents further grain refinement, owing to the lack of driving force for nucleation.

As the inverse pole figure (IPF) maps (from normal axis) show, increased holding time favors the activation of recrystallization processes, leading to grain size refinement and the formation of equiaxed α grains (Fig. 4(a)–(c)). With the progress of recrystallization, β grains were sub-divided into regions by α grains exhibiting different degrees of refinement (Fig. 4(d)–(f)). The recrystallized region has a random texture, indicating that recrystallization annealing contributes to improved homogeneity of the grain orientation.

3.2. 3D EBSD analysis

The HKL 3D Viewer software [32] was used to view and analyze the serial-sectioning data. A $7 \times 7 \times 7$ μm^3 volume of interest was used to represent the 3D morphology of the sample. Fig. 5(a) shows the IPF map of the α phase and the band contrast (BC) map of the β phase; Fig. 5(b) is the inverse of (a). The BC (Kikuchi image quality index), which reflects the degree of lattice distortion [33], of the α phase is larger than that of the β phase. This indicates that the retained strain energy of the α phase is larger than that of the β phase. The α grains shown in Fig. 5(c) and (d) have mean misorientations of 11.05° and 7.68°, respectively, whereas the β matrix grain (Fig. 5(e)) has a mean misorientation of 4.58°. The schematic

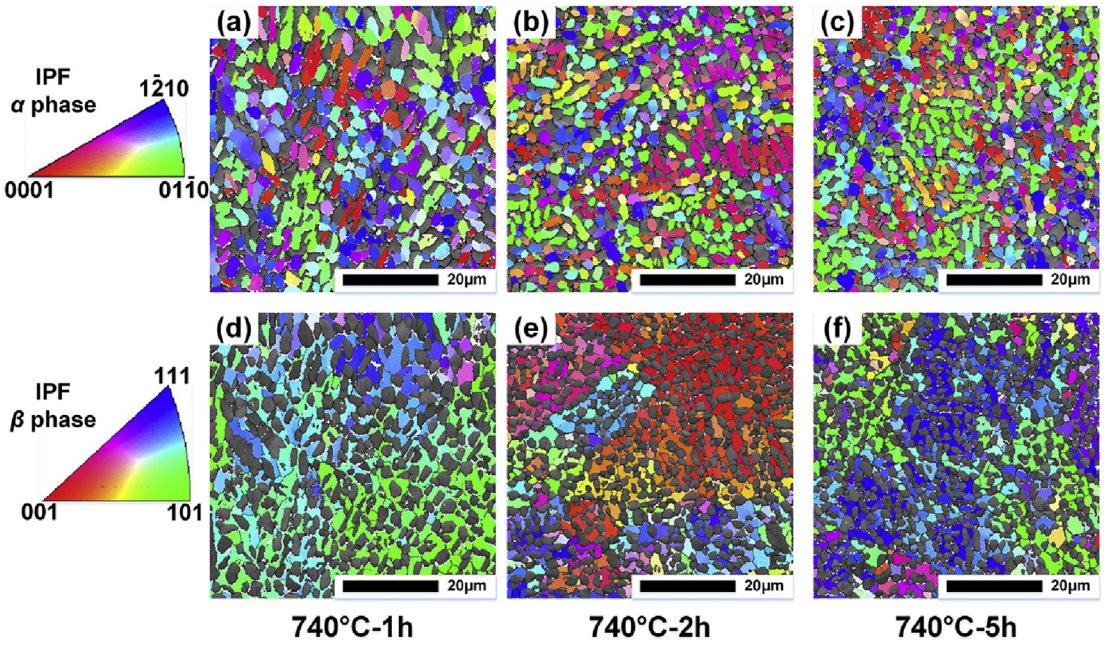

Fig. 4. IPF maps of the α phase (**(a)**–**(c)**) and β phase (**(d)**–**(f)**) in samples annealed at 740 °C for 1 h, 2 h, and 5 h.

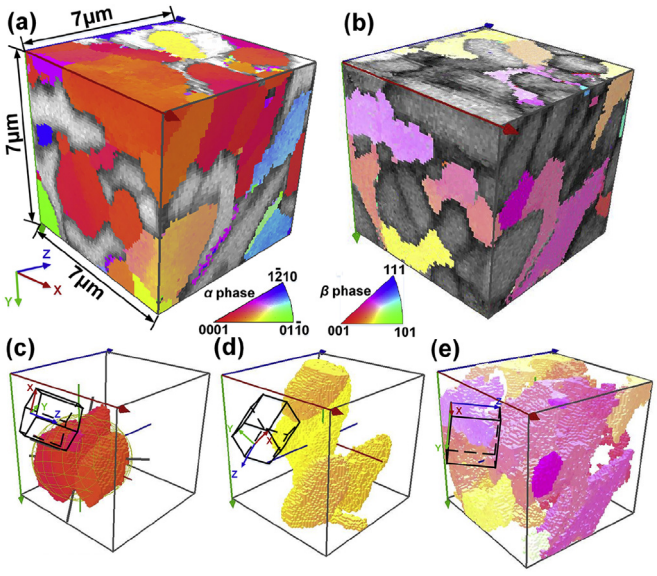

Fig. 5. **(a)** IPF map of the α phase and BC map of the β phase; **(b)** IPF map of the β phase and BC map of the α phase; 3D microstructure of **(c)** and **(d)** α grains; **(e)** a β matrix grain.

hexagons and cubes, which showed the mean crystallographic orientation of these grains, were superimposed on the maps. The 3D observations revealed that large α grains were further refined to globular and equiaxed sub-grains during recrystallization annealing and the β grains were divided into sub-regions (i.e., large matrix grains with small misorientation). This suggests that the spatial microstructure is composed of a highly globular, homogeneous, and equiaxed α phase dispersed in a sub-structured β matrix.

In this work, the morphological parameters were also successfully captured by using 3D Viewer, which processes the orientation information from the EBSD dataset and automatically segments grains by analyzing discrete changes in local orientation. The grain size may be described in terms of the equivalent-sphere diameter. The α phase has a mean equivalent-sphere diameter of 0.75 μm. Furthermore, the α and β phases have 7.76 and 19.05 mean number of neighboring grains, respectively; this parameter is useful in evaluating grain growth characteristics and grain-to-grain interactions. The misorientation angle of each grain, which is useful in calculating the orientation distribution function profile, stress intensities, and crack nucleation and growth, can also be measured.

4. Conclusions

A Ti-5.5Mo-7.2Al-4.5Zr-2.6Sn-2.1Cr titanium alloy was subjected to various periods of recrystallization annealing and the resulting microstructural evolution was characterized. The higher recrystallization rate and larger recrystallization fraction of the β phase, compared with those of the α phase, were attributed to the high strain energy storage during large deformation forging. However, the nucleation of recrystallization was prevented, owing to the high recrystallization fraction of the β phase. The 3D FIB–EBSD technique was used to reveal the spatial distribution of the microstructure comprising the alloy heat-treated at 740 °C for 5 h. The results revealed that this microstructure was composed of refined, equiaxed, and homogeneously oriented α grains dispersed in sub-structured β matrix grains.

Acknowledgment

This work was support by the Chinese National Natural Science Foundation [grant number 51571031] and the International Graduate Exchange Program of the Beijing Institute of Technology. The authors would like to thank Dr. Xiaohua Chen of the University of Science and Technology Beijing for helping to incorporate the HKL Nordlys F system into the serial-sectioning methodology.

References

[1] F.J. Humphreys, M. Hatherly, Recrystallization and Related Annealing Phenomena, second ed., Elsevier, , Oxford, 2004.
[2] T. Sakai, H. Miura, A. Goloborodko, O. Sitdikov, Continuous dynamic recrystallization during the transient severe deformation of aluminum alloy 7475,

Acta Mater. 57 (2009) 153–162.
[3] J. Huang, Z. Xu, Evolution mechanism of grain refinement based on dynamic recrystallization in multiaxially forged austenite, Mater. Lett. 60 (2006) 1854–1858.
[4] Y. Ning, Z. Yao, H. Guo, M.W. Fu, Structural-gradient-materials produced by gradient temperature heat treatment for dual-property turbine disc, J. Alloy Compd. 557 (2013) 27–33.
[5] Y. Ning, C. Zhou, H. Liang, M.W. Fu, Abnormal flow behavior and necklace microstructure of powder metallurgy superalloys with previous particle boundaries (PPBs), Mater. Sci. Eng. A 652 (2016) 84–91.
[6] G. Lütjering, Influence of processing on microstructure and mechanical properties of (α+β) titanium alloys, Mater. Sci. Eng. A 243 (1998) 32–45.
[7] K.L. Wang, M.W. Fu, S.Q. Lu, X. Li, Study of the dynamic recrystallization of Ti-6.5Al-3.5Mo-1.5Zr-0.3Si alloy in β-forging process via finite element method modeling and microstructure characterization, Mater. Des. 32 (2011) 1283–1291.
[8] D.L. OuYang, M.W. Fu, S.Q. Lu, Study on the dynamic recrystallization behavior of Ti-alloy Ti-10V-2Fe-3V in β processing via experiment and simulation, Mater. Sci. Eng. A 619 (2014) 26–34.
[9] S.L. Semiatin, S.L. Knisley, P.N. Fagin, D.R. Barker, F. Zhang, Microstructure evolution during alpha-beta heat treatment of Ti-6Al-4V, Metall. Mater. Trans. A 34 (2003) 2377–2386.
[10] S. Zhu, H. Yang, L.G. Guo, X.G. Fan, Effect of cooling rate on microstructure evolution during α/β heat treatment of TA15 titanium alloy, Mater. Charact. 70 (2012) 101–110.
[11] Z. Shi, H. Guo, J. Han, Z. Yao, Microstructure and mechanical properties of TC21 titanium alloy after heat treatment, Trans. Nonferr. Metal. Soc. 23 (2013) 2882–2889.
[12] H.K.S. Rahoma, X.P. Wang, F.T. Kong, Y.Y. Chen, J.C. Han, M. Derradji, Effect of (α+ β) heat treatment on microstructure and mechanical properties of (TiB+ TiC)/Ti–B20 matrix composite, Mater. Des. 87 (2015) 488–494.
[13] D. Qin, Y. Lu, D. Guo, L. Zheng, Q. Liu, L. Zhou, On preparation of bimodal Ti–5Al–5V–5Mo–3Cr–0.4 Si (Ti-5553s) alloy: α+ β forging and heat treatment, Mater. Sci. Eng. A 609 (2014) 42–52.
[14] X. Peng, H. Guo, Z. Shi, C. Qin, Z. Zhao, Microstructure characterization and mechanical properties of TC4-DT titanium alloy after thermomechanical treatment, Trans. Nonferr. Metal. Soc. 24 (2014) 682–689.
[15] M. Meng, H. Yang, X.G. Fan, S.L. Yan, A.M. Zhao, S. Zhu, On the modeling of diffusion-controlled growth of primary alpha in heat treatment of two-phase Ti-alloys, J. Alloy Compd. 691 (2016) 67–80.
[16] A.A. Popov, A.G. Illarionov, S.L. Demakov, S.I. Stepanov, M.S. Karabanalov, O.A. Elkina, Effect of heat-treatment conditions on structural and phase transformations in a two-phase α+ β titanium alloy subjected to thermo-mechanical treatment, Phys. Met. Metallogr. 109 (2010) 655–661.
[17] H. Jiang, P. Dong, S. Zeng, B. Wu, Effects of recrystallization on microstructure and texture evolution of cold-rolled Ti-6Al-4V alloy, J. Mater. Eng. Perform. (2016) 1–8.
[18] Y.B. Chun, S.L. Semiatin, S.K. Hwang, Monte Carlo modeling of microstructure evolution during the static recrystallization of cold-rolled, commercial-purity titanium, Acta Mater. 54 (2006) 3673–3689.
[19] L.A. Giannuzzi, F.A. Stevie, A review of focused ion beam milling techniques for TEM specimen preparation, Micron 30 (1999) 197–204.
[20] T.T. Sheng, G.P. Goh, C.H. Tung, L.F. Wang, Precision transmission electron microscopy sample preparation using a focused ion beam by extraction method, J. Vac. Sci. Technol. B 15 (1997) 610–613.
[21] B.J. Inkson, M. Mulvihill, G. Möbus, 3D determination of grain shape in a FeAl-based nanocomposite by 3D FIB tomography, Scr. Mater. 45 (2001) 753–758.
[22] M.D. Uchic, M.A. Groeber, D.M. Dimiduk, J.P. Simmons, 3D microstructural characterization of nickel superalloys via serial-sectioning using a dual beam FIB-SEM, Scr. Mater. 55 (2006) 23–28.
[23] M.A. Groeber, B.K. Haley, M.D. Uchic, 3D reconstruction and characterization of polycrystalline microstructures using a FIB-SEM system, Mater. Charact. 57 (2006) 259–273.
[24] M.D. Uchic, M.A. Groeber, D.M. Dimiduk, J.P. Simmons, 3D microstructural characterization of nickel superalloys via serial-sectioning using a dual beam FIB-SEM, Scr. Mater. 55 (2006) 23–28.
[25] M.D. Uchic, M. Groeber, R. Wheeler IV, F. Scheltens, D.M. Dimiduk, Augmenting the 3D characterization capability of the dual beam FIB-SEM, Microsc. Microanal. 10 (2004) 1136–1137.
[26] Y. Bhandari, S. Sarkar, M. Groeber, M.D. Uchic, D.M. Dimiduk, S. Ghosh, 3D polycrystalline microstructure reconstruction from FIB generated serial sections for FE analysis, Comp. Mater. Sci. 41 (2007) 222–235.
[27] S.V. Prasad, J.R. Michael, T.R. Christenson, EBSD studies on wear-induced subsurface regions in LIGA nickel, Scr. Mater. 48 (2003) 255–260.
[28] D.J. Rowenhorst, A. Gupta, C.R. Feng, G. Spanos, 3D Crystallographic and morphological analysis of coarse martensite: combining EBSD and serial sectioning, Scr. Mater. 55 (2006) 11–16.
[29] J. Konrad, S. Zaefferer, D. Raabe, Investigation of orientation gradients around a hard Laves particle in a warm-rolled Fe 3 Al-based alloy using a 3D EBSD-FIB technique, Acta Mater. 54 (2006) 1369–1380.
[30] N. Zaafarani, D. Raabe, R.N. Singh, F. Roters, S. Zaefferer, Three-dimensional investigation of the texture and microstructure below a nanoindent in a Cu single crystal using 3D EBSD and crystal plasticity finite element simulations, Acta Mater. 54 (2006) 1863–1876.
[31] S.V. Zherebtsov, G.A. Salishchev, R.M. Galeyev, Formation of sub-microcrystalline structure in titanium and its alloy under severe plastic deformation, Defect Diffus. Forum 208–209 (2002) 237–240.
[32] HKL Channel 5 3D viewer. Oxford instruments nanotechnology tools.
[33] S.I. Wright, M.M. Nowell, EBSD image quality mapping, Microsc. Microanal. Off. J. Microsc. Soc. Am. Microbeam Anal. Soc. Microsc. Soc. Can. 12 (2006) 72–84.